Wind and waves in extreme hurricanes

Leo H. Holthuijsen,[1] Mark D. Powell,[2] and Julie D. Pietrzak[1]

Received 15 February 2012; revised 8 June 2012; accepted 12 July 2012; published 1 September 2012.

[1] Waves breaking at the ocean surface are important to the dynamical, chemical and biological processes at the air-sea interface. The traditional view is that the white capping and aero-dynamical surface roughness increase with wind speed up to a limiting value. This view is fundamental to hurricane forecasting and climate research but it has never been verified at extreme winds. Here we show with observations that at high wind speeds white caps remain constant and at still higher wind speeds are joined, and increasingly dominated, by streaks of foam and spray. At surface wind speeds of ∼40 m/s the streaks merge into a white out, the roughness begins to decrease and a high-velocity surface jet begins to develop. The roughness reduces to virtually zero by ∼80 m/s wind speed, rendering the surface aero-dynamically extremely smooth in the most intense part of extreme (or major) hurricanes (wind speed > 50 m/s). A preliminary assessment shows that cross swell, dominant in large regions of hurricanes, allows the roughness under high wind conditions to increase considerably before it reduces to the same low values.

Citation: Holthuijsen, L. H., M. D. Powell, and J. D. Pietrzak (2012), Wind and waves in extreme hurricanes, *J. Geophys. Res.*, *117*, C09003, doi:10.1029/2012JC007983.

1. Introduction

[2] Breaking waves are nowhere more evident than in tropical cyclones. With climate models suggesting an increase in the frequency of intense hurricanes [*Bender et al.*, 2007], greater understanding of processes at the ocean-atmosphere interface is urgently required to improve predictions. Breaking waves create white caps, send droplets into the air, generate turbulence and exchange gases with the atmosphere. All these affect the Earth's heat budget, the mixing of the upper ocean, and the concentration of greenhouse gases. Breaking waves are therefore critically important to air-sea interactions and to modeling the Earth's climate [*Anguelova and Webster*, 2006]. They have been studied in the field [e.g., *Ross and Cardone*, 1974; *Monahan and Ó Muircheartaigh*, 1980; *Holthuijsen and Herbers*, 1986; *Kraan et al.*, 1996; *Sugihara et al.*, 2007; *Callaghan et al.*, 2008a, 2008b; *Kleiss and Melville*, 2011] but always for wind speeds <23 m/s when breaking waves appear as white caps but related manifestations such as streaks and white-out are almost absent.

[3] A breaking wave creates a patch of active foam at its crest – the white cap. As the wave moves on, the leading edge of the white cap follows the breaking crest but the trailing edge remains stationary and is slowly replaced by submerged bubbles in wind-aligned streaks. At very high wind speeds the white cap is blown off the crest in a layer of spray droplets. Under such conditions, the ocean-atmosphere interface is a foam, spray, bubble emulsion layer, which acts as a slip layer for the wind, rather than as a liquid surface [*Powell et al.*, 2003; *Emanuel*, 2003]. At very high wind speeds this layer covers the waves as a high-velocity white sheet, resulting in white out conditions.

[4] Such evolution of the surface affects the momentum transfer between the ocean and the atmosphere as shown by theory [*Kudryavtsev and Makin*, 2007; *Bye and Wolff*, 2008; *Soloviev and Lukas*, 2010] and in laboratory flumes [*Donelan et al.*, 2004; *Reul et al.*, 2008]. However, laboratory flumes are one-dimensional whereas the open ocean is two-dimensional and lateral phenomena such as cross swell, meandering and flow convergence cannot be reproduced. This is a serious shortcoming as cross swell in the open ocean shortens the crest lengths of the waves [*Longuet-Higgins*, 1957] and therefore reduces the width of the white caps and hence the intensity of related processes [*Phillips*, 1985]. This would affect the transfer of momentum between the ocean and atmosphere, and the generation of white caps and streaks.

[5] The transfer of momentum is usually formulated in terms of the wind stress $\tau = \rho_a C_D U_{10}^2$ in which the drag coefficient C_D represents the surface roughness, ρ_a is the air density and U_{10} is the wind speed at 10 m elevation. The conventional assumption is that the drag coefficient C_D increases linearly with wind speed. This has been borne out by field observations at low to moderate wind speeds [*Smith and Banke*, 1975; *Garratt*, 1977; *Large and Pond*, 1981; *Wu*, 1982; *Petersen and Renfrew*, 2009]. But at high wind speeds the value of C_D levels off and at still higher wind speeds it decreases [*Powell et al.*, 2003; *Jarosz et al.*, 2007; *Black et al.*, 2007], probably as an effect of the slip layer

[1]Environmental Fluid Mechanics Section, Faculty of Civil Engineering and Geosciences, Delft University of Technology, Delft, Netherlands.
[2]Atlantic Oceanographic and Meteorological Laboratory, National Oceanographic and Atmospheric Administration, Miami, Florida, USA.

Corresponding author: L. H. Holthuijsen, Environmental Fluid Mechanics Section, Faculty of Civil Engineering and Geosciences, Delft University of Technology, Stevinweg 1, NL-2628 CN, Delft, Netherlands. (l.h.holthuijsen@tudelft.nl)

©2012. American Geophysical Union. All Rights Reserved.
0148-0227/12/2012JC007983

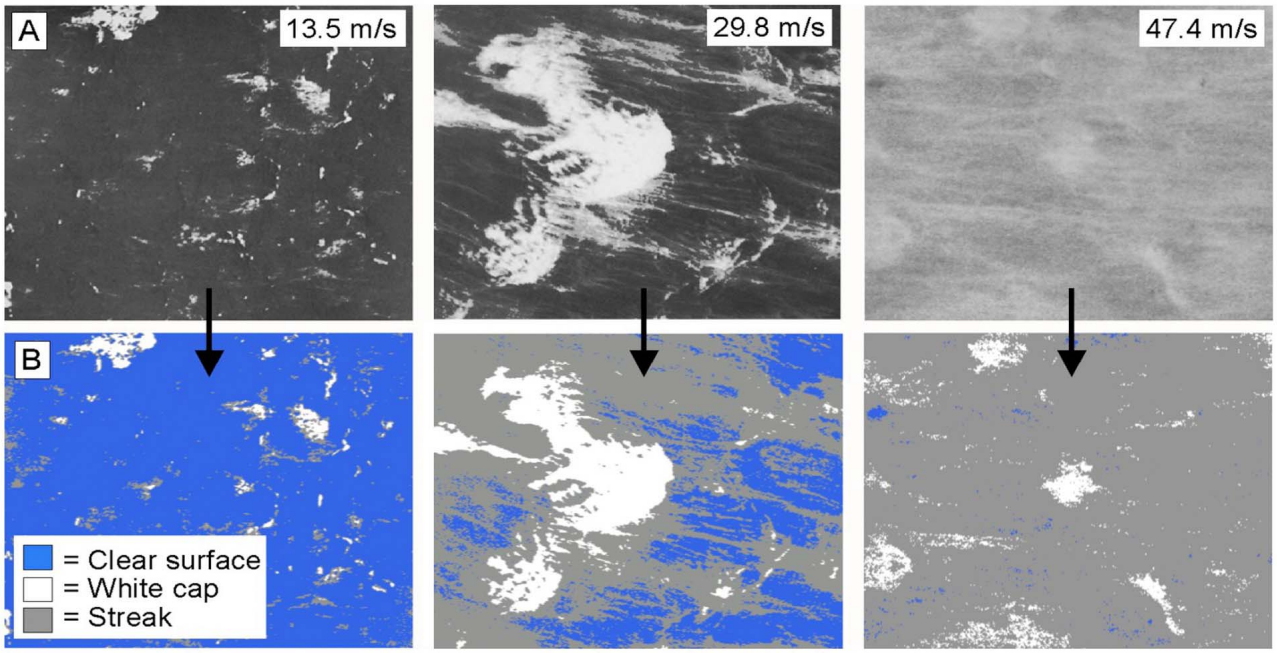

Figure 1. Three sample frames of white caps and streaks under medium to extreme wind speed conditions. (a) Black-and-white (gray tone) frames from low-level air reconnaissance flights in hurricanes (fourth-order two-dimensional trends in gray tone removed; resulting gray tones normalized between 0 – darkest - and 255 - lightest). (b) White caps and streaks identified from Figure 1a as white and gray against blue background. Pictures were taken (left to right) from 159 m, 234 m and 453 m altitude. The estimated surface wind speed (10 m elevation) is indicated.

created by white caps and streaks. Here we investigate this process using aerial reconnaissance films and GPS drop sondes in hurricanes under extreme conditions (0–500 m mean boundary layer wind speed U_{MBL} up to 90 m/s). We concentrate on wind speeds $U_{MBL} > 25$ m/s, when the white caps are joined by streaks, and eventually - at extreme wind speeds - merge into a white out (Figure 1). We then investigate the effects of cross swell. Using a numerical wave model, we show that cross swell introduces an unexpected horizontal asymmetry in hurricanes.

2. Data Collection and Processing

2.1. Wind Profiles and Drag Coefficient

[6] The wind drag coefficients that we analyzed were taken from 1149 high-resolution wind profiles collected with GPS drop sondes [*Hock and Franklin*, 1999] in the 1998–2005 NOAA Hurricane Field Programs over the Atlantic. These were obtained at distances $2 < R < 400$ km from the hurricane centers. The profiles are summarized in Figure 2 in seven groups of mean boundary layer wind speed $20 \le U_{MBL} \le 89$ m/s at 10 m/s interval. A total of 447 of these have never been published before and the number of wind profiles in winds $U_{MBL} \ge 70$ m/s has increased from 25 [*Vickery et al.*, 2009] to 107.

[7] In all groups, except the highest, the observations follow the normal logarithmic profile. This is not the case in the highest group of $80 \le U_{MBL} \le 89$ m/s which contains 26 profiles. From each group except the last, we determined the corresponding value of C_D from the roughness length z_0 which characterizes the aerodynamic surface roughness. This roughness length was obtained by extrapolating the logarithmic group profiles between 20 m and 160 m height to the fictitious zero wind speed [*Powell et al.*, 2003].

[8] Such estimation of the drag coefficient from log wind profiles assumes the existence of a constant flux layer subject to an idealized horizontal homogeneity and steady state conditions as mentioned in the *Tennekes* [1973] derivation of the log law. Observations [*French et al.*, 2007] have shown the near-constant flux layer assumption to be valid in hurricanes in winds up to $U_{10} < 28$ m/s based on eddy covariance measurements. Unfortunately those types of measurements in hurricanes are no longer possible due to low-level flight safety precautions. Such data are therefore not available for higher wind speeds. *Tennekes* [1973] states, in discussing the practical nature of the log law: "We conclude that the accuracy of the log law is not at all comparable to the accuracy of the constant-stress assumption." As regards horizontal homogeneity, there are of course, radial pressure gradients and the sondes translate over the ocean while descending. By grouping sondes with similar mean boundary layer wind speeds, the resulting mean wind profiles are representative of similar pressure gradients and surface sea state conditions, hence approaching the ideal of horizontal homogeneity. To compare the C_D values thus obtained from our wind profiles with C_D values in previous studies, we compiled the results of eight earlier, authoritative studies.

[9] The observations in the $80 \le U_{MBL} \le 89$ m/s group are indicative of a high-velocity surface jet, possibly related to intermittent high air velocities above high wave crests or thick foam layers. Thermodynamic measurements from the GPS sondes show potential temperature profiles consistent

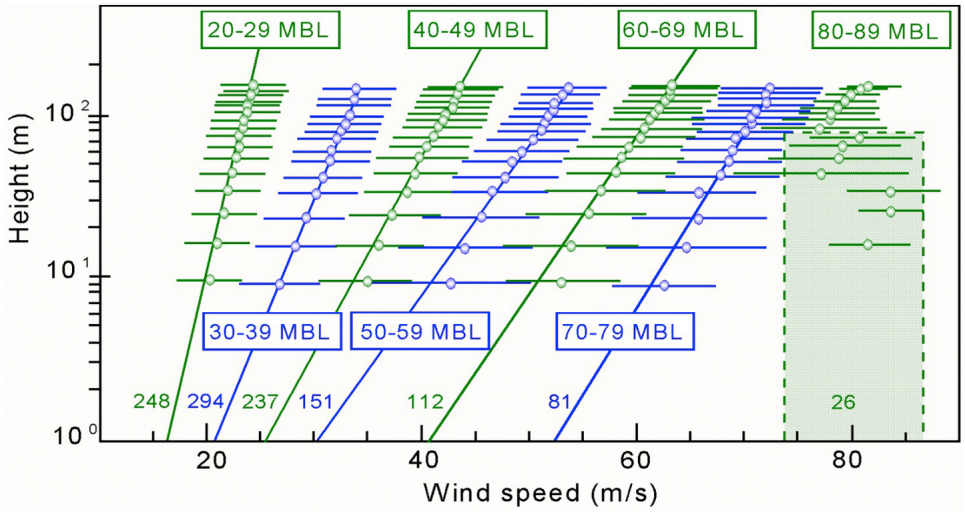

Figure 2. Mean hurricane wind profiles by mean boundary layer (MBL) wind speed group. Symbols and horizontal bars represent bin mean wind speed and one standard deviation of the observations (left and right). Inclined lines are least squares-fit lines between 20 and 160 m height. Dashed box indicates high-velocity surface jet. Numbers at the bottom of the profiles indicate number of profiles in the group.

with a relatively shallow ~100 m deep, near saturated (relative humidity 95%), well-mixed layer for this group.

2.2. Wind Field and Swell Orientation

[10] In order to investigate the influence of cross swell on the wind drag, we follow *Black et al.* [2007] who distinguish in the radar altimetry wave observations of *Wright et al.* [2001] in hurricane Bonnie (1998) three azimuthal sectors with different types of swell. Consider for the sake of exposition a hurricane in the Northern hemisphere moving northward (Figure 3). The winds rotate CCW around the hurricane eye. The highest wind speeds occur in the NE quadrant near the radius-to-maximum-wind where they generate the highest waves. When generated at a southern location at a somewhat earlier time, these high waves propagate as (young) swell (a) to the NE of the eye as following swell, (b) to the NW of the eye as cross swell and (c) to the S of the eye as opposing swell. Some high frequency (slow traveling) swell may be retained as cross swell in the area southeast of the eye. Waves from other parts of the hurricane radiate away from the hurricane.

[11] The observations in Bonnie of *Wright et al.* [2001, Figures 12, 13, and 14], which we re-plot in Figure 4a, confirm this generic pattern. We attributed to each of these observations one of the swell types which, following *Donelan et al.* [1997] and *Sugihara et al.* [2007], we define as following swell when it travels within 45° from the wind direction, cross swell when it travels within 45° from the normal to the wind direction and opposing swell when it travels within 45° from the opposing direction. In addition we distinguish a near field (near the radius-to-maximum-wind) and a far field (farther away from the center). The result is given in Figure 4b.

[12] We thus find that in the near field (near the radius-to-maximum-wind), and therefore at high wind speeds, cross swell dominates the left-front sector, opposing swell dominates the rear sector and following swell dominates the right-front sector. Farther afield, and therefore at lower wind speeds, cross swell dominates practically everywhere (except to the right-hand side of the eye). *Hu and Chen* [2011] show with large scale buoy observations averaged over 7 hurricanes, a far field pattern that is similar to the near field pattern of Bonnie and consistent with the secondary and tertiary wavefields of *Wright et al.* [2001].

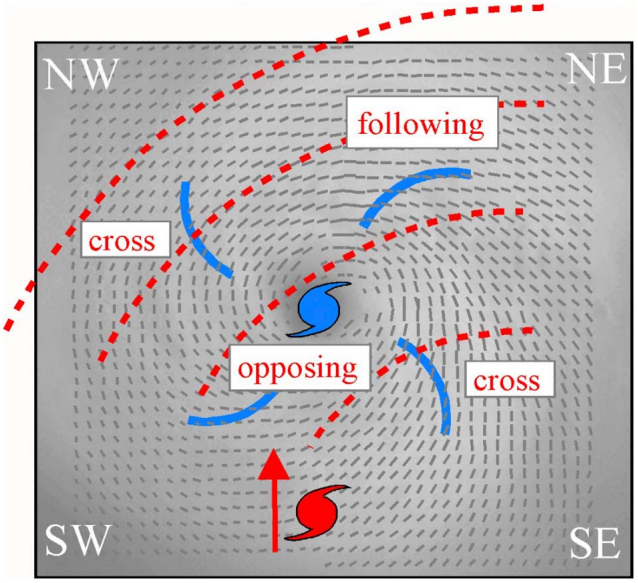

Figure 3. The swell types in a hypothetical hurricane in the Northern hemisphere moving northward. Blue symbol shows the eye. Red symbol shows the eye at a location to the south somewhat earlier in time. Blue curved lines indicate locally generated wind sea. Red curved lines indicate (young) swell generated at the southern location dispersing away from that location. Following swell occurs where red and blue lines indicate same direction of propagation (NE of eye), cross swell occurs where red and blue lines cross (NW and SE of eye) and opposing swell occurs where red and blue lines indicate opposite direction of propagation (S of eye).

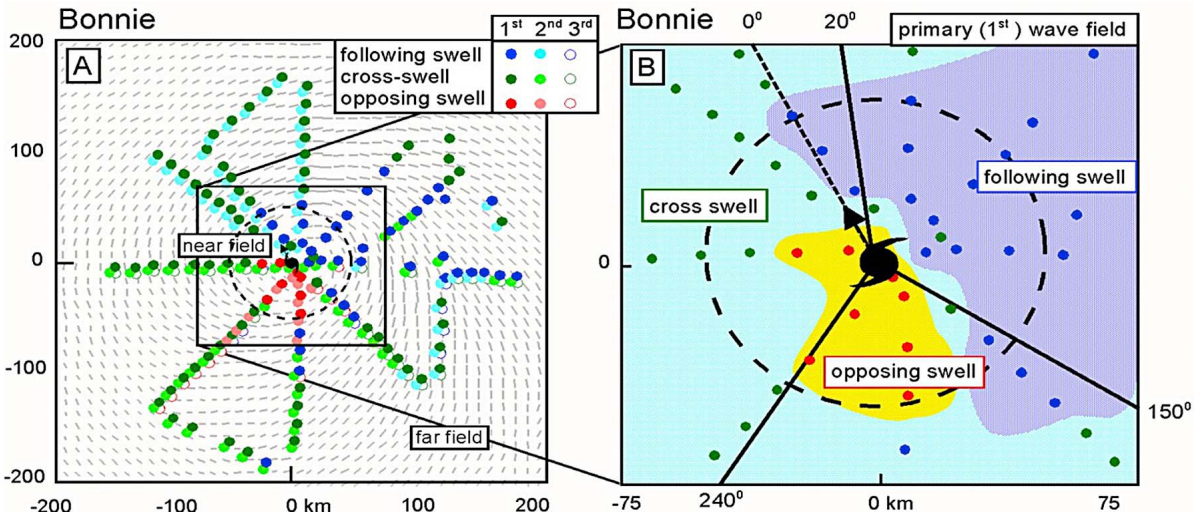

Figure 4. Following, crossing and opposing swell in hurricane Bonnie inferred from *Wright et al.* [2001]. (a) The swell character of the primary wavefield (1st), the secondary wavefield (2nd) and the tertiary wavefield (3rd) in the near and far field. Every second data point from the original data set removed for reasons of presentation. Wind field suggested in background by gray vectors. Radius-to-maximum-wind indicated with dashed circle. (b) The distribution of swell character of the primary (1st) wavefield in the near field – from the distribution in Figure 4a, and the three azimuthal sectors proposed by *Black et al.* [2007] superimposed.

[13] We sorted our C_D values of Figure 2 in each wind speed group (except the highest) over the three azimuthal sectors. To avoid the eye of the hurricanes, with poorly defined wind and wave directions, we removed observations closer than 30 km from the center. For the purpose of a preliminary assessment, these observations can be approximated with an analytical function in terms of the wind speed and a number of tunable coefficients:

$$C_D \times 10^3 = \min\{[a + b(U_{10}/U_{\mathrm{ref},1})^c], d[1 - (U_{10}/U_{\mathrm{ref},2})^e]\} \quad (1)$$

[14] The spread of the data around this approximation was relatively large and we did not attempt a formal fit to the data. Instead, a visual fit provided the values of the coefficients (with a strong bias to previous studies for $U_{10} < 30$ m/s in view of the large number of observations in these studies). This emphasizes the preliminary nature of this approximation.

2.3. White Caps and Streaks

[15] The films that we used to estimate the coverage of the ocean surface with white caps and streaks were taken in hurricanes Ella (1978), Greta (1978), Inez (1966), Ellen (1973), Eloise (1975), Gladys (1975) and Gloria (1976). In addition we had access to frames of films taken in hurricanes David (1979) and Allen (1980). These films (from the files of the National Oceanographic and Atmospheric Administration, Atlantic Oceanographic and Meteorological Laboratory, Miami, USA) were taken with nadir-looking cameras during low-level flights (100 m–1500 m) with eye-wall penetrations at 150–450 m altitude. This was dangerous and such flights have been discontinued as a safety precaution. The films are therefore unique and will probably remain so for the foreseeable future. We analyzed the 86 frames - 5 on average for each Beaufort category ranging from 3 to 19 - which *Black and Adams* [1983] selected from hurricanes Eloise, Gladys, Allen and David in the context of estimating sea state winds by observers during low level reconnaissance flights. They considered these images to be representative of the ocean surface appearance under moderate to extreme wind conditions with surface wind speed between 7 m/s and 50 m/s (at 20 m elevation). We therefore analyzed, perforce, a fair number of selected frames and not a large sample of each wind/wave condition as recommended by *Callaghan et al.* [2008b].

[16] In an initial visual inspection, we distinguished four features in these frames, which we illustrate here with one frame in Figure 5. (1) White caps are the white, geometrically coherent patches of foam at the crest of breaking waves. The aspect ratio (width: height = along crest: normal to crest) of these white caps is typically between 1 and 2. The trailing edge may be ragged to the point of shedding up-wind trails of the same brightness. Although the frame rates in the films did not capture the lifecycle of individual white caps, we surmise the following (partly based on direct visual observations of the second author). (2) While the trailing edge of the white cap (including any detached trails) is dissolving in the wake of the breaking wave, the entrained air rises to the surface, creating streaks of bubbles. The aspect ratio of this patch is typically ~1 but of the individual streaks it varies from ~1 to well under 1/10 (i.e., narrow streaks in the wind direction). (3) When the white cap is blown off the crest at high wind speeds, it generates spray flying downwind just above the water, hitting the water in the troughs or in the back of down-wind waves. These streaks are much finer and meander downstream (like snow blowing above pack snow). Occasionally the source of such a streak is seen to be a white cap at its up-wind end but usually the streaks are free from any white cap. (4) At very high wind speeds, the white caps, the spray and the streaks disperse into a semi-transparent

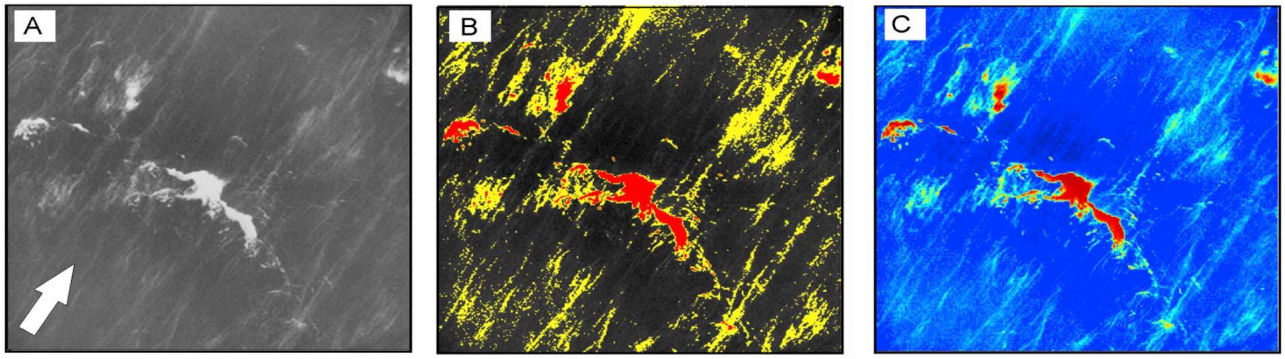

Figure 5. Three versions of one sample film frame of the ocean surface during hurricane Gladys (flight level 330 m; estimated wind speed ~30 m/s at 10 m elevation). (a) Black-and-white (gray tone) frame; fourth-order 2D trends in gray tone removed; resulting gray tones normalized between 0 – darkest - and 255 - lightest. Estimated wind direction (from streak direction and white cap curvature) indicated with arrow. (b) White caps and streaks identified with three discrete colors: red and yellow against black back ground. (c) Continuous false-color version of Figure 5a.

high-velocity sheet of mist – the white out. The mist gets denser (visually) to practically opaque as the wind speed (at 10 m elevation) approaches 40 m/s. In the analysis we combine the coverage of white caps and their trails into "white cap coverage" and the coverage by the streaks into "streak coverage."

[17] The images of *Black and Adams* [1983] were available as black-and-white (actually gray tone) prints and our analysis is similar to that of *Kraan et al.* [1996], *Sugihara et al.* [2007], *Lafon et al.* [2004, 2007], *Callaghan and White* [2009] and *Kleiss and Melville* [2011] in that we used gray tone thresholds to define features in the images. The published procedures use one threshold to distinguish white caps from the clear sea surface. We tried to introduce an addition second threshold in an automated procedure to also distinguish streaks but we failed, possibly because streaks are more diffusive features than white caps (Figure 5). Instead, we visually inspected each frame individually. We scanned the prints at high resolution (2400 dpi) and a computer script generated 3 versions. The first is a de-trended normalized version. The de-trending consisted of removing a 4th–order 2D polynomial from the gray tones in the image to remove uneven lighting conditions (including vignetting effects; Figure 5a). The resulting gray tones were then normalized to a value 0 for the darkest tone and 255 for the lightest tone. The second version was created by assigning three discrete colors (red, yellow and black) to three gray tones separated by two (controllable) thresholds. For each image, these thresholds were chosen visually to identify white caps and streaks (Figure 5b). The relative number of red pixels provided the white cap coverage W; the relative number of yellow pixels provided the streak coverage S (after clipping to remove the border each image contained a total of approximately 360 × 360 pixels). The third version of the image was obtained as a false color image of the first version (continuous color range red, orange, yellow, cyan and blue; Figure 5c). This version was used to distinguish vaguely visible features as possible white caps or streaks, particularly in the darker regions of the original frame. All frames were first analyzed by all three authors three times independently and finally once jointly. The white cap coverages (W) and the streak coverages (S) of the final analysis were averaged over 2 m/s wind speed intervals. Four frames were removed because of poor lighting conditions (2x) or the presence of clouds (2x). We computed for each image the statistical distribution of gray tones (number of pixels as a function of threshold level) and its first- and second-order derivatives to the threshold level but, in contrast to the earlier studies referred to above with similar methods, we found the shape of these functions generally too ambiguous to identify the threshold levels that visually defined white caps and streaks.

[18] *Black and Adams* [1983] estimated the winds by providing the 30-s average flight level winds and the estimated surface air-sea temperature differences to a planetary boundary layer model [*Powell*, 1980; *Black and Adams*, 1983]. We re-analyzed the wind speeds > 20 m/s through an iterative procedure starting with a first guess for the roughness length (computed from C_D for that 20 m wind speed), and then using equation 5 from *Vickery et al.* [2009] with the flight-level wind speed to estimate friction velocity, and a 10 m wind speed, and then repeating the steps to estimate a final 10 m wind speed. For lower wind speeds, we used the average ratio (0.915) between the wind speed at 20 m elevation and at 10 m elevation thus obtained.

[19] We plotted the bin mean values of white cap coverages (W) and streak coverages (S) as a function of wind speed U_{10}. Following previous white cap studies [e.g., *Monahan and Ó Muircheartaigh*, 1980; *Callaghan*, 2008a, 2008b] we approximated our observed values of W with a power law $W = aU_{10}^b$. We estimated the coefficients with a least squares regression in the wind speed range over which the white cap coverage seemed to increase, which is coincidentally the same as the range of observations of previous studies ($U_{10} \leq$ 24 m/s, Section 3). At higher wind speeds we see no systematic dependency on wind speed. At these wind speeds, the values of W seem to fluctuate around a low constant value which we estimated as the arithmetical mean of these values. The corresponding transition from the lower wind speeds to the higher wind speeds, with an overshoot, is tentatively approximated using a tanh limiter $W = c \tanh \{aU_{10}^b/c\}$ with a variable $c = d - e \tanh \{f(U_{10} - U_{ref})\}$ (no relation with the coefficients of equation (1)). The

coefficients of this expression were estimated with a visual fit to the data.

[20] The streak coverage increased rapidly with increasing wind speed, suggesting an exponential growth toward full saturation. We therefore used the exponential function $S = \alpha \exp(\beta U_{10})$ and we determined the coefficients α and β with a least squares technique in the wind speed range of rapid growth ($U_{10} \leq 26$ m/s) above which the streak coverage seemed to converge to full saturation. To represent this convergence, we limit S with a tanh limiter $S = \gamma \tanh \{\alpha \exp(\beta U_{10})\}$ such that the sum of white cap and streak coverage is unity at very high wind speeds (white out conditions).

2.4. Wave Directional Spreading

[21] The definition of three azimuthal sectors by *Black et al.* [2007] was based on partitioning the two-dimensional wave spectra of *Wright et al.* [2001] to identify peaks in the bi-modal or multimodal shape of the spectra. Such partitioning can be carried out by an inspection of every individual spectrum, as was done by *Wright et al.* [2001] or with an automated procedure [*Hanson and Phillips*, 2001; *Portilla et al.*, 2009]. In either case, the attribution of swell type is discrete (following, opposing or cross swell). The sorting in geographic space over the three azimuthal sectors is also discrete. This is unsatisfactory as the physical processes that affect the wind drag are locally defined and do not vary discontinuously with swell type in spectral space nor in geographic space and do not depend on the direction of motion of the hurricane. We argued above that the relevant parameter is the change in crest length rather than swell type.

[22] The normalized crest length λ can be defined as the ratio of the mean zero-crossing wavelength in the mean wave direction (for definition, see Appendix A) over the equivalent length normal to that direction i.e., along the crest [*Longuet-Higgins*, 1957] $\lambda = (m_{2,0}/m_{0,2})^{1/2}$ in which $m_{2,0}$ and $m_{0,2}$ are the two principal second-order moments of the wave number spectrum. It is directly related to the wave directional spreading $\lambda^2 = 1/\sigma_\theta^2 - 1$ in which the wave directional spreading is defined as $\sigma_\theta = \langle \sin^2(\theta) \rangle^{1/2}$ with θ relative to the mean wave direction and the $\langle\ \rangle$ operator indicating the average over spectral direction weighted with energy density [*Battjes*, 1972]. For a locally generated spectrum without swell, typically $\sigma_\theta \sim 30°$ [*Holthuijsen*, 2007, p. 163]. If a swell spectrum is added that is identical to a locally generated spectrum but propagating at 90° across the wind direction, the (normalized) crest length reduces considerably from typically $\lambda = 1.7$ to $\lambda = 1$, while the value of σ_θ increases to $\sigma_\theta \sim 67°$. Opposing swell continues increasing the value to $\sigma_\theta \sim 81°$ but returns the crest length to its original value (by virtue of the circular character of the directional energy distribution). The definition of σ_θ implies that swell is accounted for in proportion to its energy relative to the energy of the locally generated waves. It has the added advantage of being readily and efficiently predicted with numerical wave prediction models. It also gives a continuous grading of swell type and it varies as a continuous variable in geographic space.

[23] To determine the relationship between σ_θ and the three azimuthal sectors and possibly any correlation between white capping and streak generation, we used the numerical SWAN wave model [*Booij et al.*, 1999]. We simulated the waves in two hurricanes with reasonably straight tracks as was the case for Bonnie (1998): Luis (1995) and Fran (1996). In the SWAN model the waves are represented with the directional wave spectrum as a function of geographic location and time. For each individual wave component of this spectrum, a Eulerian energy balance accounts for wave propagation (linear theory for surface gravity waves), generation by wind (linear and exponential growth), dissipation by wave breaking (based on the mean wave steepness) and nonlinear wave-wave interactions (resonant quadruplet interactions). We integrated this balance with a frequency resolution of 10% and a directional resolution of 15° on a 0.25° × 0.25° geographic grid over the western North Atlantic Ocean to determine the wave spectrum every 15 min at every grid point. The directional spreading is computed from the spectrum as $\sigma_\theta = \langle 4 \sin^2(\frac{1}{2}\theta) \rangle^{1/2}$ as suggested by *Kuik et al.* [1988]. Other computed wave (related) parameters are defined in Appendix A. It is relevant in view of our use of SWAN to note that (a) we did not modify SWAN, (b) the dissipation by whitecapping in SWAN is independent of any wave directional characteristic (as in other third-generation wave models such as the WAM model [*WAMDI group*, 1988] or the WAVEWATCH model [*Tolman and Chalikov*, 1996]) and (c) we used simulated wind fields of the hurricanes computed independently of the present study (see Acknowledgments). The main purpose was to obtain realistic wind and wavefields for our analysis.

[24] We could thus relate the geographic distribution of the computed σ_θ to the three azimuthal sectors and establish a relationship between our sorted values of C_D and σ_θ. With such a relationship C_D can be estimated from locally defined values of σ_θ and U_{10} in any arbitrary wind and wavefield, including that of a hurricane, without reference to the location or direction of motion of the hurricane.

3. Results

[25] An overview of the eight earlier, authoritative studies of the drag coefficient that we consider is given in Table 1. Several of these studies include data from older studies in this set. We removed this overlap: if an older study and a younger study shared the same data, then these were removed from the younger study. Occasionally this was not possible because such data were included in the published averages of a study. Details are summarized in Table 1.

[26] The C_D values from these studies and from our wind profiles of Figure 2 are given in Figure 6a as a function of surface wind speed U_{10} (except for the anomalous wind profile group $80 \leq U_{MBL} \leq 89$ m/s). For high wind speeds ($40 < U_{10} < 50$ m/s) our data are consistent with previous GPS sonde data [*Powell et al.*, 2003] and balance estimates [*Jarosz et al.*, 2007]. The very low value $C_D = 0.7 \times 10^{-3}$ at very high wind speeds ($U_{10} \approx 60$ m/s in Figure 6a) seems inconsistent with white out conditions in which the layer of foam needs to be sustained. However, white out need not be associated with a high drag coefficient. It is sufficient to have a high wind speed. Once the foam is there, it is plausible that the drag goes down, and the momentum transfer needed to maintain the foam depends on the half-life of the foam. If that is large, not much momentum and energy transfer is needed to maintain it (K. Hasselmann, personal communication, 2012). For wind speeds $U_{10} < 40$ m/s our values are considerably lower than those in the previous studies. At lower wind speeds and therefore in the far field of

Table 1. Previous Studies of the Wind Drag Coefficient[a]

Study	Number of Data Sets Minus Number of Data Sets Removed (Reason)	Method (Number of Retained Data Sets) Averaged Over Wind Speed Bin
Smith and Banke [1975, Figure 3]	3 minus 1 (surf zone)	ec (2), 2 m/s[b]
Garratt [1977, Figure 3]	14, *Garratt* [1977, Figure 4] in *Wu* [1982, Figure 1]	ec (8), wp (6), 2 m/s[b]
Large and Pond [1981, Figure 6]	1	d and ec (1), 1.5–3 m/s
Wu [1982, Figure 1]	9 minus 1 (hurricanes partially over land [*Miller*, 1964])	gd (1), amb (2), wp (2), d (2), ec (2)
Powell et al. [2003, Figure 3]	7 minus 6 (earlier studies)	wp (1), averaged over four height layers[b]
CBLAST [*Black et al.*, 2007; Figure 5]	1	ecp
Jarosz et al. [2007, Figure 3]	2 minus 1 (earlier study and *Powell et al.* [2003])	omb (1), 2 m/s[b]
Petersen and Renfrew [2009, Figure 8]	5 minus 1 (CBLAST)	ec (2), id (1), 1 m/s (per data set, if ≥10 data points per bin), 2 m/s[b] for SOWEX data of *Banner et al.* [1999, Figure 8]

[a]The first column identifies the studies in the compilation. The second column gives the number of data sets minus the number of data sets that have been removed from the study in the first column, and the reason for the removal. The third column gives the method of observation that was used in the data sets retained (with the number of data sets per method) and the width of the wind speed bin over which the C_D values of the retained data sets were averaged. Abbreviations: ec = eddy correlation, ecp = eddy correlation profile, wp = wind profile, d = dissipation, gd = geostrophic departure, amb = atmospheric momentum balance, omb = ocean momentum balance, id = inertial dissipation.

[b]By present authors.

the hurricanes, the presence of cross swell may have reduced the wind drag (see below). This seems consistent with swell induced reduction of white capping at low wind speeds $U_{10} <$ 13 m/s [*Sugihara et al.*, 2007; *Callaghan et al.*, 2008b]. We also note that for these wind speeds our values lie within the large scatter of the previous studies. To illustrate this, we plotted in Figure 7 the observations in 7 hurricanes of *Black et al.* [2007]. These C_D values were estimated by extrapolating to the surface, eddy correlation measurements at different flight levels. Their estimates include C_D values that are similar to ours under the same wind conditions in the same storms (personal information from the second author, MDP), although the process of extrapolating to the surface introduces additional uncertainty to the normally accurate eddy correlation method. *Black et al.* [2007] sorted these observations over the quadrants of the hurricanes (Figure 7) although information of the left-rear quadrant is not available in *Black et al.* [2007]. A linear regression through the data shows that the C_D values tend to be higher to the right of the hurricane eye (presumably dominated by following and opposing swell) than in the left-front quadrant (presumably dominated by cross swell) with diminishing differences toward $U_{10} = 30$ m/s.

[27] Our C_D values sorted over the azimuthal sectors, or equivalently, the type of swell, are shown in Figure 6b. For wind speeds $U_{10} < 25$ m/s approximately, these values are considerably lower in the left-front sector (cross swell) than in the right front and rear sectors (following swell or opposing swell) with diminishing differences toward $U_{10} = 30$ m/s as in the observations of *Black et al.* [2007] in Figure 7. Swell therefore seems to reduce the wind drag at these wind speeds and more so under cross swell conditions than under following or opposing swell conditions. The effects of following swell and opposing swell are otherwise uncertain. *Donelan et al.* [1997, Figure 9] see in their wind observations $U_{10} < 15$ m/s, swell increasing C_D, irrespective of the type of swell. *Drennan et al.* [1999] in their low wind observations $U_{10} < 8$ m/s, see following swell decreasing C_D. It may be noted that, although the relation between white capping and wind drag is tenuous, swell under low wind conditions $U_{10} < 13$ m/s seems to also reduce white capping [*Sugihara et al.*, 2007; *Callaghan et al.*, 2008b] but *Goddijn-Murphy et al.* [2011] see no such effect under higher wind conditions $8.6 < U_{10} < 23.1$ m/s.

[28] At higher wind speeds $U_{10} > 30 \sim 35$ m/s, under following or opposing swell conditions, our C_D values level off at $C_D \approx 2 \times 10^{-3}$ (Figure 6b). However, under cross swell conditions our C_D values continue increasing to $C_D \approx 5 \times 10^{-3}$ before decreasing to the same value. Under these wind conditions, cross swell apparently postpones the reduction of the wind drag, possibly by postponing the creation of the foam-spray slip layer. This maximum value is high but it is based on 38 wind profiles (with 44 wind samples in the 25 m height bin) and therefore statistically reliable (as shown by the 90% confidence interval in Figure 6b). Moreover, *Taylor and Yelland* [2001] show with observations that $z_0/H_s = 1200(H_s/L_p)^{4.5}$ (L_p is the peak wavelength in the wave spectrum) which indicates that with wave steepness $H_s/L_p = 0.60 - 065$ and significant wave height H_s = 14–15 m as computed with SWAN in hurricanes Luis and Fran (maximum values under same conditions as in Figure 9), a roughness length z_0 as high as $z_0 = 0.05$ m, or equivalently, a drag coefficient of $C_d = 7 \times 10^{-3}$ seems attainable in any major hurricane. The absence of sorted observations for $U_{10} > 50$ m/s indicates that not enough wind speed samples at distances to hurricane center $R > 30$ km were available at each height bin for a reasonable estimate of the mean profile.

[29] The overall result for extreme wind speeds is that at distances to hurricane center $R > 30$ km (Figure 6b) the azimuthally sorted data tend to reach a limiting value of about $C_d = 2 \times 10^{-3}$, whereas for $R < 30$ km (Figure 6a), with winds $60 \leq U_{MBL} \leq 79$ m/s, much lower C_d values are evident e.g., $C_d = 0.7 \times 10^{-3}$ at surface wind speeds over 60 m/s. Since the most intense storms tend to have smaller radii of maximum wind speeds, the very low limiting values tend to be located in the vicinity of the eye wall, where waves are extremely fetch limited and the continuous breaking mechanism [*Donelan et al.*, 2004] can contribute to enhanced foam generation.

[30] For a preliminary assessment, our C_D values (sorted for $U_{10} < 50$ m/s and unsorted for $U_{10} > 50$ m/s), together

with the data from the previous studies in Figure 6b, can be approximated with the expression of equation (1) using the coefficients of Table 2 for all wind speeds, with and without cross swell.

[31] Figure 6c shows that the white cap coverage as we observed it, initially increases to a maximum at U_{10} = 24 m/s only to decrease again to a limiting value. At the higher wind speeds the white caps are joined, and increasingly dominated, by streaks with the streak coverage S growing rapidly to full saturation in white out conditions.

[32] In all earlier studies [*Goddijn-Murphy et al.*, 2011; *Callaghan et al.*, 2008a, 2008b; *Anguelova and Webster*, 2006, and references therein] except *Nordberg et al.* [1971] and *Ross and Cardone* [1974], such streaks were either

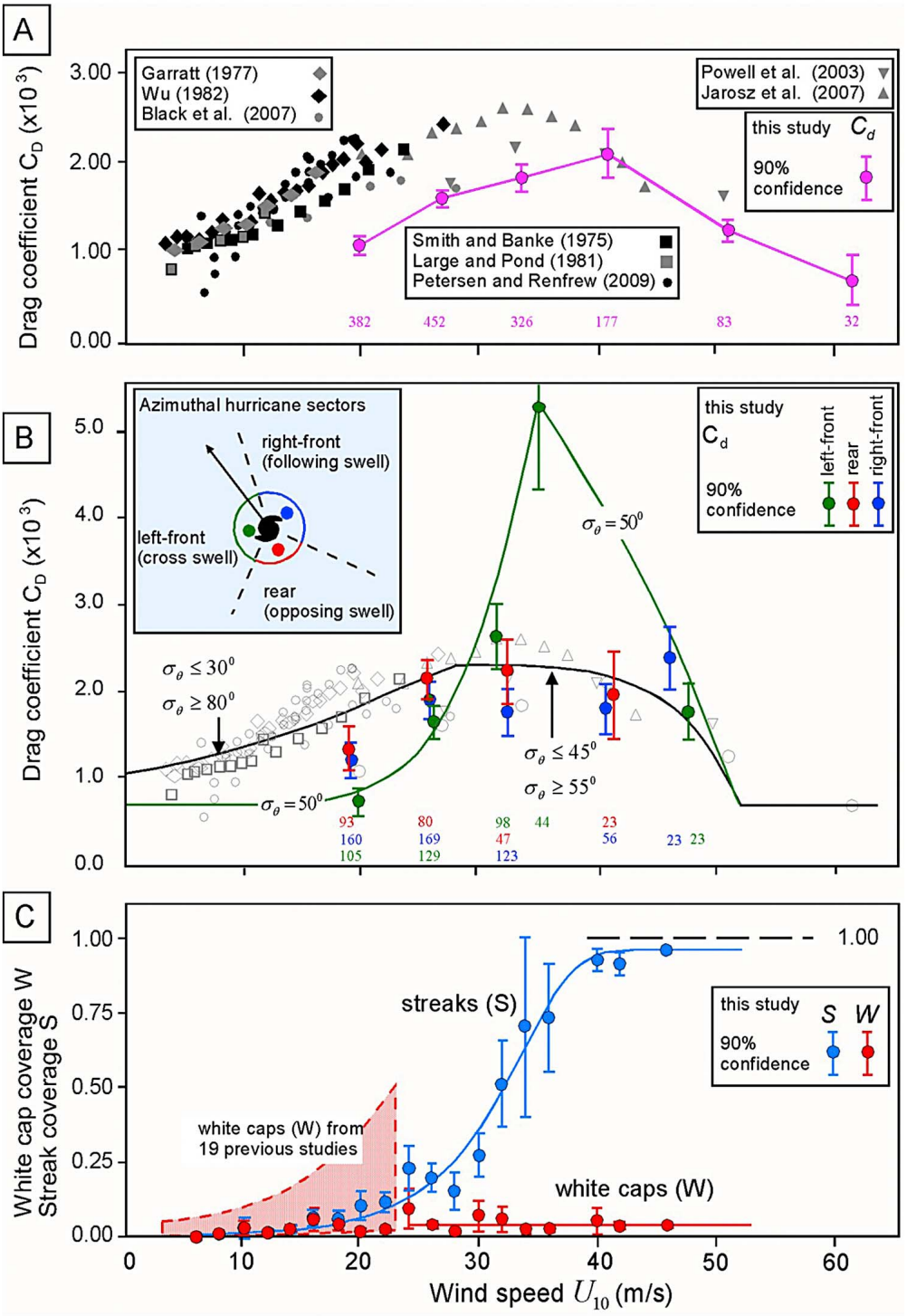

Figure 6

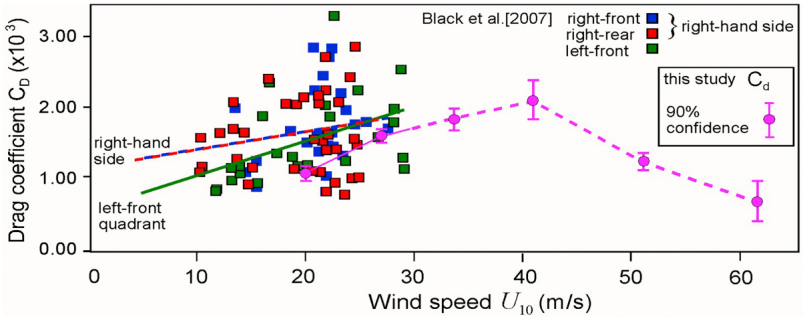

Figure 7. The scatter in the sorted observations of *Black et al.* [2007] and the bin mean observations of the present study (from Figure 6a). The straight lines are least squares fits through the observations on the right-hand side of the hurricanes and the left front quadrant. The observations of the present study are shown with the broken line (solid in the range of comparison and dashed outside this range).

ignored or processed as white caps presumably because in all these studies (in situ) wind speeds $U_{10} < 23$ m/s and streaks were few and not well defined. Moreover, these observations were often made at an oblique angle from a platform at relatively low altitude, which may have made the streaks – if present - less visible. Also, the analysis techniques that were used in these studies did not distinguish between white caps and streaks. This may explain, at least in part, the large diversity in the estimates of the white cap coverage W in these studies shown in Figure 6c [*Anguelova and Webster*, 2006]. Other reasons for the diversity may be statistical sample variability or the influence of other physical parameters than the wind speed, such as wave age, sea state, swell, ambient currents, temperature and salinity.

[33] The studies of *Nordberg et al.* [1971] and *Ross and Cardone* [1974] seem to be the first in which white caps and streaks were analyzed as separate features. The white cap coverage in these studies (in which $9.5 < U_{10} < 23.1$ m/s) fluctuates at higher wind speeds around a fairly low value slightly above $W = 0.05$. In the observations of *Callaghan et al.* [2008a] and *Goddijn-Murphy et al.* [2011], the value of W increases from $W \approx 0.01$ at $U_{10} = 10$ m/s with a decreasing rate of change to $W \approx 0.05$ at $U_{10} = 27.5$ m/s, suggesting a convergence to a slightly higher value.

[34] The least squares fit of the power law $W = aU_{10}^b$ through our bin mean observations for $U_{10} \leq 24$ m/s (the range of wind speeds over which white cap coverage increases; Figure 8) resulted in $a = 4 \times 10^{-6}$, $b = 3.12$ but with a fairly large degree of uncertainty (the coefficient of determination $R^2 = 0.603$). Such (near) cubed dependency of the white cap coverage on the wind speed agrees well with earlier observations [*Zhao and Toba*, 2001; *Anguelova and Webster*, 2006; *Sugihara et al.*, 2007; *Callaghan et al.*, 2008a; *Goddijn-Murphy et al.*, 2011]. Figure 8 also shows that our results are almost identical to those of *Callaghan et al.* [2008a] which are based on considerably more observations and less scatter (and $U_{10} \leq 23$ m/s). However, it must be noted that in view of the large scatter in our observations, this agreement is rather surprising. For $U_{10} > 24$ m/s, up to the maximum observed wind speed $U_{10} = 46$ m/s, we see no systematic dependency of our observations on the wind speed. They fluctuate around $W = 0.04$ with a relatively high scatter, the standard deviation being $\sigma_W = 0.02$.

[35] Taken over the full wind speed range, our observations seem to imply that the white cap coverage does not converge monotonically from low values to a limiting higher value. It overshoots the limiting value by almost a factor 2. Whether this behavior is physically real, for instance streaks being generated at the expense of white capping, or that it reflects a problem in the analysis of our film frames, for instance the visual identification of white caps being affected by the appearance of streaks is open to speculation (but we do not expect a factor 2). A very tentative approximation which includes the overshoot is achieved with the tanh limiter $W = c \tanh \{aU_{10}^b/c\}$ with a variable $c = d - e \tanh \{f(U_{10} - U_{ref})\}$ with $d = 10$, $e = 6$, $f = 0.5$ and $U_{ref} = 26$ m/s (Figure 8).

Figure 6. Bin mean values of observed drag coefficient C_D, white cap coverage W and streak coverage S as a function of surface wind speed U_{10}. (a) Magenta symbols represent the C_D observation of the present study derived from the average wind profile in each of 6 wind speed classes U_{MBL} = 20(10)80 m/s, at distances to hurricane center $2 < R < 400$ km. Gray symbols represent observations from previous studies (indicated in insets). (b) Open gray symbols are identical to those in Figure 6a (including this study). Solid colored symbols are the C_D observations of the present study sorted over azimuthal hurricane sectors (inset; the direction of hurricane motion is indicated with an arrow; azimuthal sector boundaries clockwise at 20°, 150° and 240° relative to motion direction) for distances to hurricane center $R > 30$ km. The solid green line represents the analytical approximation for cross swell (at $\sigma_\theta = 50°$) and the solid black line for following and opposing swell ($\sigma_\theta \leq 30°$ and $\geq 80°$ at wind speeds $U_{10} < 27.5$ m/s; and $\sigma_\theta \leq 45°$ and $\geq 55°$ at wind speeds $U_{10} \geq 27.5$ m/s) and the C_D values of the previous studies. (c) Blue and red dots represent bin mean of the observations of this study for each 2 m/s wind speed bin. Shaded area represents white cap coverage W from 19 previous studies (compiled by *Anguelova and Webster* [2006, Figure 1]), curved blue line represents analytical approximation, horizontal red line represents mean value for $U_{10} > 24$ m/s. Vertical bars represent 90% confidence interval of mean value. Numbers at the bottom indicate sample sizes used in computing the data points with the same color directly above as determined by the number of wind speed measurements in the 25 m height bin.

Table 2. The Coefficients of Equation (1) to Approximate the C_D Values in Figure 6b and the Suggested Validity in Terms of Wave Directional Spreading[a]

No Swell, Opposing Swell, Following Swell	Cross Swell
$U_{ref,1}$ = 27.5 m/s	
a = 1.05, b = 1.25, c = 1.4; $\sigma_\theta \le 30°$ or $\sigma_\theta \ge 80°$	a = 0.7, b = 1.1, c = 6; $\sigma_\theta = 50°$
$U_{ref,2}$ = 54 m/s	
d = 2.3, e = 10; $\sigma_\theta \le 45°$ or $\sigma_\theta \ge 55°$	d = 8.2, e = 2.5; $\sigma_\theta = 50°$

[a]Lower limit $C_D = 0.7 \times 10^{-3}$.

[36] Our observed streak coverage S grows exponentially from ~0.07 at 20 m/s wind speed to full saturation at ~40 m/s wind speed when white out occurs. The rapid increase of this coverage as a function of wind speed in the presence of a constant white cap coverage (which of course is a simplification, Figures 6 and 8) is readily explained as a cumulative effect. If the production of streaks were constant and if the life span of a streak would increase with wind speed, then the streak coverage would also increase with wind speed. The result of fitting the capped exponential growth $S = \gamma \tanh\{\alpha \exp(\beta U_{10})\}$ to these observations is shown as the solid blue line in Figure 6c with $\alpha = 0.00175$, $\beta = 0.18$ and $\gamma = 0.96$. When comparing these results with the evolution of the drag coefficient, it is obvious that the onset of the drag coefficient leveling off coincides with the onset of the creation of streaks at $U_{10} \approx 25$ m/s.

[37] The correlation between our C_D values and the type of swell (and thus presumably its effect on white capping and streak generation) is demonstrated with the relation between the three azimuthal sectors and the wave directional spreading as seen in our wave hindcasts of hurricanes Luis and Fran (Figure 9).

[38] We found that in the near field, as long as the hurricanes are far removed from land, the boundaries of the three azimuthal sectors correspond well with the 45° and 55° contour lines of the wave directional spreading. In the near-field right-front sector (following swell) we find $\sigma_\theta \le 45°$, in the near-field rear sector (opposing swell) $\sigma_\theta \ge 55°$ and in the near-field left-front sector (cross swell) $45° < \sigma_\theta < 55°$. Cross swell also occurs in a narrow zone between the right-front sector and the rear sector where the following swell turns into an opposing swell. These results provide the range of validity of the approximation of equation (1) and its coefficients of Table 2 in terms of the wave directional spreading. When using this approximation at other values of the wave directional spreading than those mentioned here, the coefficient values can be linearly interpolated to obtain the C_D values.

[39] Other wave parameters may be relevant as an alternative or as supplementary to the wave directional spreading [*Donelan et al.*, 1993; *Kraan et al.*, 1996; *Callaghan et al.*, 2008b]. We therefore also inspected the geographic patterns of the significant wave height H_s, the wave steepness s, the wave dissipation by white capping S_{wc}, the energy transfer from wind to waves S_{wind}, the inverse wave age $U_{10}^{\parallel}/c$ and the (absolute) difference between wind and wave direction $|\Delta\theta|$. The definitions and the results for hurricane Luis are given in Appendix A. The results were essentially the same for hurricane Fran (not shown here). The patterns of the significant wave height, steepness, white capping and wind energy transfer resemble a comma wrapped around the hurricane eye, with the highest values in the right front sector diminishing gradually to the left front sector. The distinction between the right front sector and the left front sector is not as clear as in the pattern of the wave directional spreading σ_θ (Figure 9). The patterns of the inverse wave age $U_{10}^{\parallel}/c$ and the absolute difference between wind and wave direction $|\Delta\theta|$ are similar to the pattern of the wave directional spreading σ_θ by virtue of their definition. A larger value of $|\Delta\theta|$ gives smaller values of $U_{10}^{\parallel}/c$ (because the wind speed component in the mean wave direction is involved) and σ_θ increases as the value of $|\Delta\theta|$ increases. These patterns may therefore potentially be used to identify swell type. However, the wave directional spreading, being based on the second-order circular moment of the directional energy distribution is more sensitive to the presence of swell (or rather, to perturbations at large angles) than the mean wave direction which is based on first-order circular moments of that distribution. Moreover, estimating the directional difference requires extra information (the wind direction) to be obtained from the wind field or from a spectral partitioning of the spectrum. Such partitioning would also be required for other wave parameters, such as the energy ratio of swell and local wind sea [*Carlsson et al.*, 2010]. Both partitioning and wind

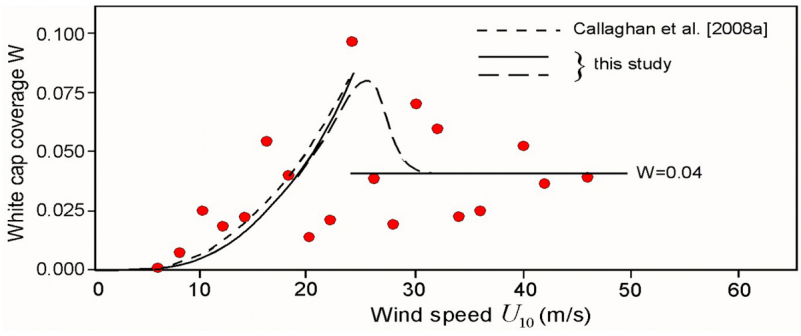

Figure 8. The white cap coverage observations of this study (also in Figure 6C) approximated with a power law for wind speeds $U_{10} \le 24$ m/s and a constant for $U_{10} > 24$ m/s (solid lines) and a tanh capping with overshoot to a limiting value (long dashes). The two power laws from *Callaghan et al.* [2008a] concatenated at $U_{10} = 10$ m/s are shown with short dashes.

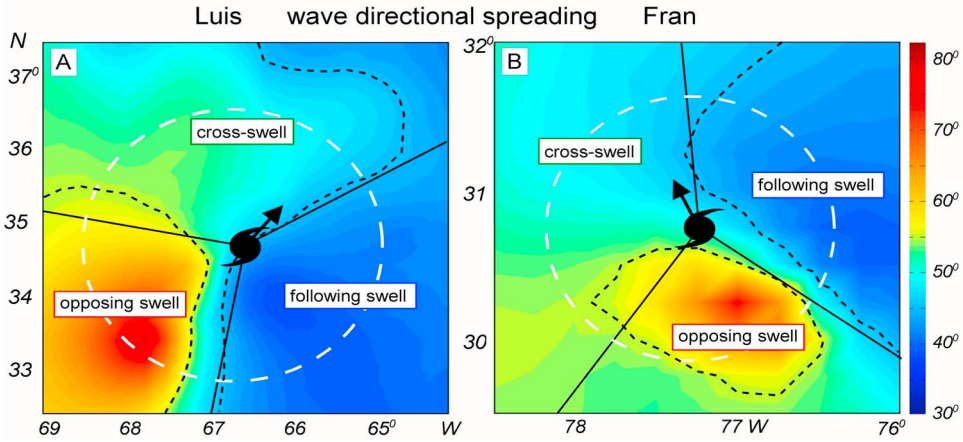

Figure 9. The geographic pattern of the computed wave directional spreading in hurricanes Luis (Sept. 10, 1995, 05:00 UTC) and Fran (Sept. 5, 1996, 15:00 UTC). The contours of wave directional spreading $\sigma_\theta = 45°$ and $\sigma_\theta = 55°$ are indicated with dashed black lines. The pale blue-green colors correspond to cross swell; the dark blue colors to following swell and the yellow-red colors to opposing swell. The azimuthal sector boundaries are indicated with black solid lines; the radius-to-maximum-wind with a white dashed circle. Black arrow indicates direction of hurricane motion.

information can be avoided by using the wave directional spreading.

4. Discussion

[40] Our observations of white caps and streaks at high wind speeds $U_{10} > 35$ m/s suggest that the horizontal distribution of the air-sea exchange of momentum, heat and moisture in real hurricanes is different from those in atmospheric models. Most tropical cyclone models [*Moon et al.*, 2007; *Gopalakrishnan et al.*, 2011] have incorporated a wind speed dependent C_D, which is capped when surface winds reach 30–35 m/s. We find that C_D levels off at such wind speeds, and then decreases to even lower values than reported earlier [*Powell et al.*, 2003] as winds strengthen to extreme values $U_{10} > 60$ m/s. In addition, we find that wind speed dependence of C_D varies spatially around the tropical cyclone in response to sea state caused by wind-swell interactions. Locations with cross swell (wave directional spreading 45°–55°) under high wind conditions experience limited breaking which contributes to larger C_D until wind speeds are high enough that the continuous breaking mechanism [*Donelan et al.*, 2004] predominates, resulting in a thick foam-spray layer with very smooth roughness properties.

[41] The leveling off of the drag coefficient and the subsequent decrease to a low limiting value coincides with the generation of streaks of foam and droplets at the surface, possibly at the expense of white caps, eventually creating white out conditions at $U_{10} > 40$ m/s. At lower wind speeds, $U_{10} < 25$ m/s our observations suggest that wind drag is reduced by swell, more so by cross swell than by opposing or following swell. This seems to occur simultaneously with reduced white capping which is also more affected by cross swell than by following swell [*Goddijn-Murphy et al.*, 2011].

[42] Modeling studies [e.g., *Emanuel*, 1995; *Bryan and Rotunno*, 2009] suggest that the maximum potential intensity of tropical cyclones is sensitive to the ratio of the enthalpy coefficient C_e to C_D, such that intense cyclones cannot be sustained unless C_e/C_D is above some threshold value, ranging from 0.25 to 1.5. While our results extend the denominator of that ratio to more extreme wind speeds, C_e is still unknown at wind speeds above 29 m/s in the field [*Drennan et al.*, 2007; *Zhang et al.*, 2008] and 38 m/s in the laboratory [*Haus et al.*, 2010].

[43] Estimating the effect of the azimuthal dependency of C_D on the wavefield is not trivial. The C_D values in the right front and rear sectors (with following or opposing swell) are barely affected by this dependency. Without other modifications to the wave energy balance, the waves would therefore be affected only to the extent that their generation in the left front sector may be affected. In the left-front sector (with cross swell) the azimuthal dependency of C_D would increase wave generation under high wind $U_{10} > 30$ m/s conditions. Under lower wind conditions $U_{10} < 30$ m/s, wave generation would be reduced. This would also be the case in the far field since cross swell seems to reduce C_D at these wind speeds. However, given the success of the wave models in predicting the significant wave height in hurricanes [*Dietrich et al.*, 2011a, 2011b, 2012; *Kennedy et al.*, 2011, for SWAN hurricane wave hindcasts], we expect that compensating modifications would be required. The prime candidate would be the dissipation by white capping which is poorly understood. At present it is represented in 3rd generation operational wave models such as SWAN as a closure term with calibrated coefficients and it does not depend on wave directional characteristics. A more thorough assessment would require modifying and coupling an atmospheric model and a wave model [*Chen et al.*, 2007] which we consider to be beyond the scope of the present study.

[44] To find a preliminary estimate of the effect of our C_D observations, we estimated the pattern of the drag coefficient C_D and the surface stress τ in a major hurricane using our parameterization of equation (1) with the coefficients of Table 2. We used the wavefield as computed with the unmodified SWAN wave model, driven by a given wind field (see Acknowledgments) of hurricane Katrina (2005).

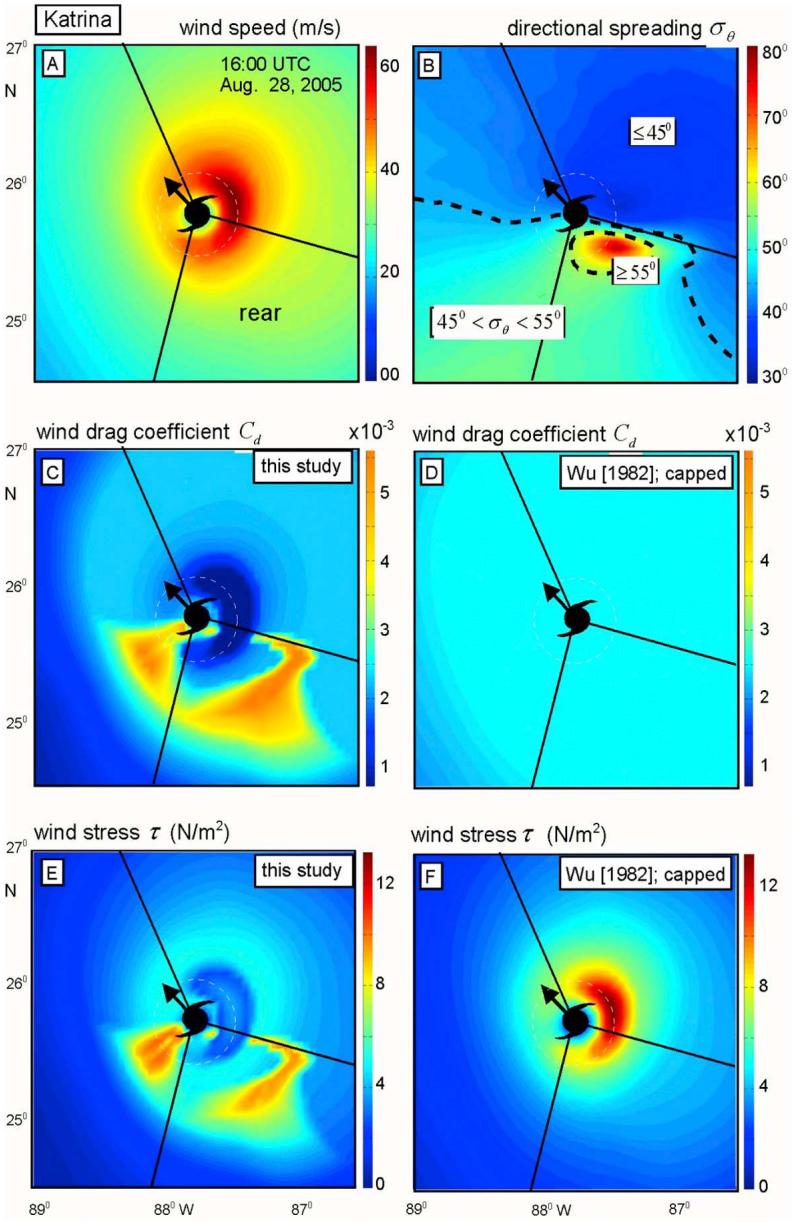

Figure 10. The geographic patterns of wind and waves in hurricane Katrina when it was at its most intense (maximum wind speed U_{10} = 64.2 m/s on Aug. 28, 2005, 16:00 UTC). (a) The wind speed. (b) The wave directional spreading computed with the SWAN wave model. (c and d) The drag coefficient as determined with the expression of equation (1) and (interpolated) coefficients of Table 2 of the present study and with the expression of *Wu* [1982] (capped at 2.5 × 10^{-3}). (e and f) The wind stress determined from the wind speed and the drag coefficients.

The surface stress is computed with the standard expression given in the Introduction. We show the results in Figure 10 when the hurricane was at its most intense (U_{10} = 64.2 m/s [*Powell et al.* [2010]). The white out, which occurs in the region with very high wind speeds (Figure 10a) creates a region with low drag coefficient to the right and immediate rear of the eye (Figure 10c). The combination of high (but not the highest) wind speeds and cross-swell, $45° < \sigma_\theta < 55°$ creates a belt of high values around the region with opposing swell, $\sigma_\theta \geq 55°$ with one maximum to the left of the eye and another in the far rear of the eye (Figure 10c). But where this belt overlaps with the white out, the values are low. The pattern of the surface stress (Figure 10e) is similar. These findings contrast sharply with the accepted view of a nearly uniform distribution of the drag coefficient under high wind conditions and a well defined maximum surface stress to the right of the eye, for instance computed with the expression for C_D of *Wu* [1982] capped at $C_D = 2.5 \times 10^{-3}$ (Figures 10d and 10f).

[45] Modifying tropical cyclone models in the sense of our results, together with the most recent C_e values will lead to higher C_e/C_D ratios and more intense storms [e.g., *Zweers et al.*, 2010]. In addition, azimuthal sea state variability may induce surface friction asymmetries that could impact

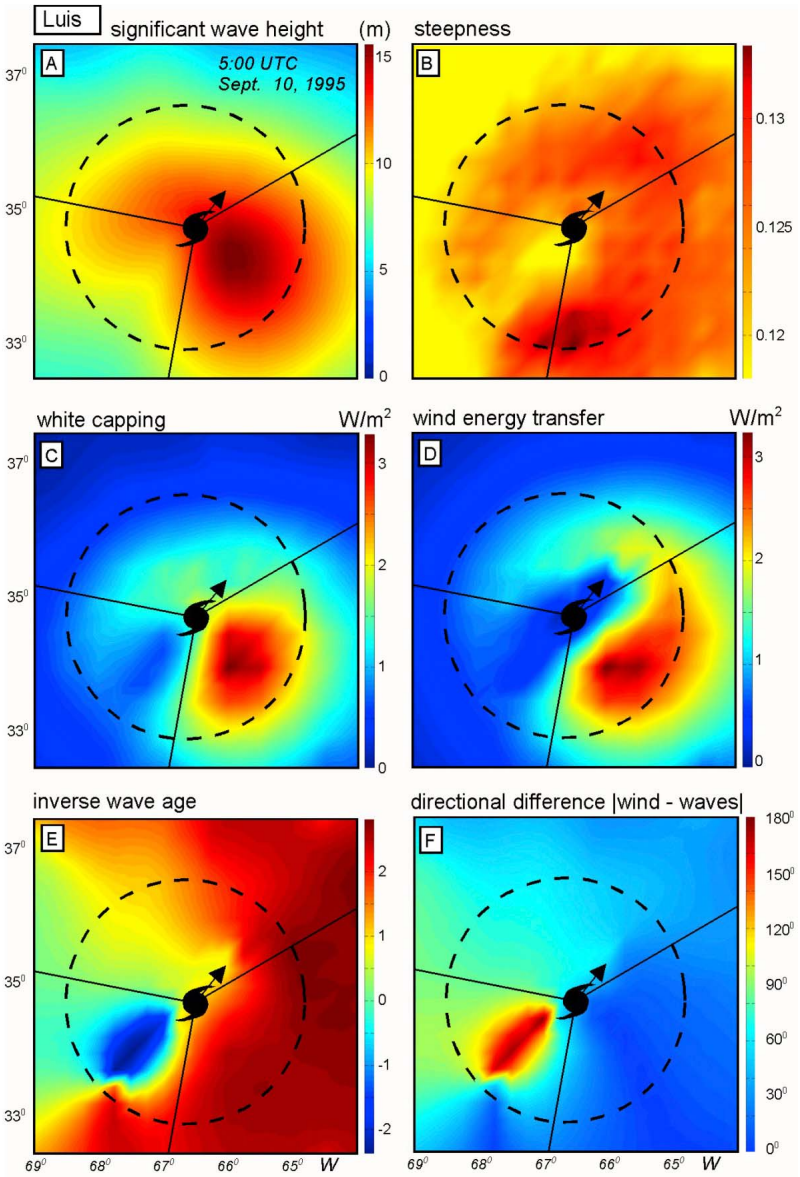

Figure A1. The geographic patterns in hurricane Luis (Sept. 10, 1995, 5:00 UTC) of the computed significant (a) wave height, (b) wave steepness, (c) white capping, (d) energy transfer from wind to waves, (e) inverse wave age and (f) the absolute difference between wind and wave direction. The azimuthal sector boundaries are indicated with black solid lines; the radius-to-maximum-wind with a white dashed circle. Black arrow indicates direction of hurricane motion.

horizontal convergence and rainband formation. These results reinforce the need to couple atmosphere, wave and ocean models to account for sea state feedbacks across the air-sea interface. This will obviously affect wind, wave and surge forecasts with corresponding implications for coastal flooding, risk assessment and disaster management.

Appendix A: The Geographic Patterns of Wave Parameters in Hurricane Luis

[46] We computed the following wave (related) parameters in hurricanes Luis and Fran with the SWAN wave model with the same wind fields as underlying Figure 9 of the main text: the significant wave height, defined as $H_{m0} = 4\sqrt{m_0}$ where m_0 is the zeroth order moment of the wave frequency spectrum, the wave steepness, defined as the significant wave height divided by the mean wavelength defined as the wavelength of the mean wave period $T_{m01} = m_0/m_1$ where m_1 is the first-order moment of the frequency spectrum (we also computed the steepness on the basis of the peak frequency but this value varied erratically, depending on the presence of multiple swell peaks), the wave dissipation by white capping defined as the integral over spectral frequency and direction of the white capping source term in the wave model, the energy transfer from wind to waves similarly defined, the inverse wave age $U_{10}^{\parallel}/c$ defined as the ratio of the wind speed in the mean wave direction $U_{10}^{\parallel}$ and the

phase velocity c of the mean wave period (this allows negative values) and the absolute difference $|\Delta\theta|$ between the wind direction and the mean wave direction (defined as $\sigma_0 = \arctan\{\langle\sin\theta\rangle/\langle\cos\theta\rangle\}$ from *Kuik et al.* [1988]). The results for hurricane Luis are shown in Figure A1. Those for hurricane Fran are essentially the same (not shown here).

[47] **Acknowledgments.** We thank the NOAA crews for producing the films during the low-level flights in the hurricanes of 1973–1980 that we inspected. We acknowledge that the frames that we analyzed were compiled by Peter Black and William Adams of the NOAA Atlantic Oceanographic and Meteorological Laboratory. We thank the U.S. Air Force and NOAA crews and scientists for collecting the GPS sonde observations (2000–2005 Hurricane Field Programs, NOAA, Office of Naval Research, National Science Foundation, NASA). We thank James Salmon and Pieter Smit (PhD students at Delft University, supported by the U.S. Office of Naval Research under grants N00014-10-1-0453 and N00014-06-1-0256, respectively) for the wave model computations and the image analysis script and Neal Dorst of NOAA for assistance with the sea state photographs. We acknowledge the support of the Joint Hurricane Testbed for a portion of the GPS sonde analysis and the assistance of Sonia Otero and Russell St. Fleur (University of Miami–NOAA Cooperative Institute for Marine and Atmospheric Studies) with the GPS sonde database. We thank Vince Cardone of Oceanweather Inc. for providing us with the wind fields. We also thank the anonymous reviewers of the manuscript for their comments which greatly helped us improving our presentation.

References

Anguelova, M. D., and F. Webster (2006), White cap coverage from satellite measurements: A first step toward modeling the variability of oceanic white caps, *J. Geophys. Res.*, *111*, C03017, doi:10.1029/2005JC003158.

Banner, M. L., W. Chen, E. J. Walsh, J. B. Jensen, S. Lee, and C. Fandry (1999), The Southern Ocean Waves Experiment. Part I: Overview and mean results, *J. Phys. Oceanogr.*, *29*(9), 2130–2145, doi:10.1175/1520-0485(1999)029<2130:TSOWEP>2.0.CO;2.

Battjes, J. A. (1972), Radiation stresses in short-crested waves, *J. Mar. Res.*, *30*(1), 56–64.

Bender, M. A., I. Ginis, R. Tuleya, B. Thomas, and T. Marchok (2007), The operational GFDL coupled hurricane-ocean prediction system and a summary of its performance, *Mon. Weather Rev.*, *135*, 3965–3989, doi:10.1175/2007MWR2032.1.

Black, P., and W. Adams (1983), Guidance for estimating surface winds based on sea state observations from aircraft and sea state catalog, *Rep. FCM-G1-1983*, 84 pp., NOAA, U.S Dep. of Commer., Washington, D. C.

Black, P. G., E. A. D'Asaro, W. M. Drennan, J. R. French, P. P. Niiler, T. B. Sanford, E. J. Terrill, E. J. Walsh, and J. A. Zhang (2007), Air-sea exchange in hurricanes: Synthesis of observations from the Coupled Boundary Layer Air-Sea Transfer Experiment, *Bull. Am. Meteorol. Soc.*, *88*(3), 357–374, doi:10.1175/BAMS-88-3-357.

Booij, N., R. C. Ris, and L. H. Holthuijsen (1999), A third-generation wave model for coastal regions, Part I, Model description and validation, *J. Geophys. Res.*, *104*(C4), 7649–7666, doi:10.1029/98JC02622.

Bryan, G. H., and R. Rotunno (2009), Evaluation of an analytical model for the maximum intensity of tropical cyclones, *J. Atmos. Sci.*, *66*, 3042–3060, doi:10.1175/2009JAS3038.1.

Bye, J. A. T., and J.-O. Wolff (2008), Charnock dynamics: A model for the velocity structure in the wave boundary layer of the air-sea interface, *Ocean Dyn.*, *58*, 31–42, doi:10.1007/s10236-007-0130-5.

Callaghan, A. H., and M. White (2009), Automated processing of sea surface images for the determination of whitecap coverage, *J. Atmos. Oceanic Technol.*, *26*(2), 383–394, doi:10.1175/2008JTECHO634.1.

Callaghan, A., G. DeLeeuw, L. Cohen, and C. D. O'Dowd (2008a), Relationship of oceanic whitecap coverage to wind speed and wind history, *Geophys. Res. Lett.*, *35*, L23609, doi:10.1029/2008GL036165.

Callaghan, A. H., G. B. Deane, and M. D. Stokes (2008b), Observed physical and environmental causes of scatter in whitecap coverage values in a fetch-limited coastal zone, *J. Geophys. Res.*, *113*, C05022, doi:10.1029/2007JC004453.

Carlsson, B., Y. Papadimitrakis, and A. Rutgersson (2010), Evaluation of a roughness length model and sea surface properties with data from the Baltic Sea, *J. Phys. Oceanogr.*, *40*(9), 2007–2024, doi:10.1175/2010JPO4340.1.

Chen, S. S., J. F. Price, W. Zhao, M. A. Donelan, and E. J. Walsh (2007), The CBLAST-Hurricane Program and the next-generation fully coupled atmosphere-wave-ocean models for hurricane research and prediction, *Bull. Am. Meteorol. Soc.*, *88*, 311–317, doi:10.1175/BAMS-88-3-311.

Dietrich, J. C., M. Zijlema, J. J. Westerink, L. H. Holthuijsen, C. Dawson, R. A. Luettich Jr., R. E. Jensen, J. M. Smith, G. S. Stelling, and G. W. Stone (2011a), Modeling hurricane waves and storm surge using integrally coupled scalable computations, *Coastal Eng.*, *58*, 45–65, doi:10.1016/j.coastaleng.2010.08.001.

Dietrich, J. C., et al. (2011b), Hurricane Gustav waves and storm surge: Hindcast, synoptic analysis, and validation in southern Louisiana, *Mon. Weather Rev.*, *139*(8), 2488–2522, doi:10.1175/2011MWR3611.1.

Dietrich, J. C., S. Tanaka, J. J. Westerink, C. N. Dawson, R. A. Luettich Jr., M. Zijlema, L. H. Holthuijsen, J. M. Smith, L. G. Westerink, and H. J. Westerink (2012), Performance of the unstructured-mesh, SWAN + ADCIRC model in computing hurricane waves and surge, *J. Sci. Comput.*, *52*(2), 468–497, doi:10.1007/s10915-011-9555-6.

Donelan, M. A., F. W. Dobson, S. D. Smith, and R. J. Anderson (1993), On the dependence of sea surface roughness on wave development, *J. Phys. Oceanogr.*, *23*(9), 2143–2149, doi:10.1175/1520-0485(1993)023<2143:OTDOSS>2.0.CO;2.

Donelan, M. A., W. M. Drennan, and K. B. Katsaros (1997), The air-sea momentum flux in conditions of wind sea and swell, *J. Phys. Oceanogr.*, *27*, 2087–2099, doi:10.1175/1520-0485(1997)027<2087:TASMFI>2.0.CO;2.

Donelan, M. A., B. K. Haus, N. Reul, W. J. Plant, M. Stiassnie, H. C. Graber, O. B. Brown, and E. S. Saltzman (2004), On the limiting aerodynamic roughness of the ocean in very strong winds, *Geophys. Res. Lett.*, *31*, L18306, doi:10.1029/2004GL019460.

Drennan, W. M., K. K. Kahma, and M. A. Donelan (1999), On momentum flux and velocity spectra over waves, *Boundary Layer Meteorol.*, *92*, 489–515, doi:10.1023/A:1002054820455.

Drennan, W. M., J. A. Zhang, J. R. French, C. McCormick, and P. G. Black (2007), Turbulent fluxes in the hurricane boundary layer. Part II: Latent heat flux, *J. Atmos. Sci.*, *64*, 1103–1115, doi:10.1175/JAS3889.1.

Emanuel, K. A. (1995), Sensitivity of tropical cyclones to surface exchange coefficients and a revised steady state model incorporating eye dynamics, *J. Atmos. Sci.*, *52*, 3969–3976, doi:10.1175/1520-0469(1995)052<3969:SOTCTS>2.0.CO;2.

Emanuel, K. (2003), A similarity hypothesis for air-sea exchange at extreme wind speeds, *J. Atmos. Sci.*, *60*, 1420–1428, doi:10.1175/1520-0469(2003)060<1420:ASHFAE>2.0.CO;2.

French, J. R., W. M. Drennan, J. A. Zhang, and P. G. Black (2007), Turbulent fluxes in the hurricane boundary layer. Part I: Momentum flux, *J. Atmos. Sci.*, *64*(4), 1089–1102, doi:10.1175/JAS3887.1.

Garratt, J. R. (1977), Review of drag coefficients over oceans and continents, *Mon. Weather Rev.*, *105*, 915–929, doi:10.1175/1520-0493(1977)105<0915:RODCOO>2.0.CO;2.

Goddijn-Murphy, L., D. K. Woolf, and A. H. Callaghan (2011), Parameterization and algorithms for oceanic whitecap coverage, *J. Phys. Oceanogr.*, *41*(4), 742–756, doi:10.1175/2010JPO4533.1.

Gopalakrishnan, S., Q. Liu, T. Marchok, D. Sheinin, N. Surgi, M. Tong, V. Tallapragada, R. Tuleya, R. Yablonsky, and X. Zhang (2011), Hurricane Weather Research and Forecasting (HWRF) model: 2011 scientific documentation, Dev. Testbed Cent., Boulder, Colo. [Available at www.emc.ncep.noaa.gov/HWRF/HWRFScientificDocumentation2011.pdf.]

Hanson, J. L., and O. M. Phillips (2001), Automated analysis of ocean surface directional wave spectra, *J. Atmos. Oceanic Technol.*, *18*(2), 277–293, doi:10.1175/1520-0426(2001)018<0277:AAOOSD>2.0.CO;2.

Haus, B. K., D. Jeong, M. A. Donelan, J. A. Zhang, and I. Savelyev (2010), Relative rates of sea-air heat transfer and frictional drag in very high winds, *Geophys. Res. Lett.*, *37*, L07802, doi:10.1029/2009GL042206.

Hock, T. R., and J. L. Franklin (1999), The NCAR GPS dropwindsonde, *Bull. Am. Meteorol. Soc.*, *80*, 407–420, doi:10.1175/1520-0477(1999)080<0407:TNGD>2.0.CO;2.

Holthuijsen, L. H. (2007), *Waves in Oceanic and Coastal Waters*, 387 pp., Cambridge Univ. Press, Cambridge, U. K., doi:10.1017/CBO9780511618536.

Holthuijsen, L. H., and T. H. C. Herbers (1986), Statistics of breaking waves observed as whitecaps in the open sea, *J. Phys. Oceanogr.*, *16*(2), 290–297, doi:10.1175/1520-0485(1986)016<0290:SOBWOA>2.0.CO;2.

Hu, K., and Q. Chen (2011), Directional spectra of hurricane generated waves in the Gulf of Mexico, *Geophys. Res. Lett.*, *38*, L19608, doi:10.1029/2011GL049145.

Jarosz, E., D. A. Mitchell, D. W. Wang, and W. J. Teague (2007), Bottom-up determination of air-sea momentum exchange under a major tropical cyclone, *Science*, *315*, 1707–1709, doi:10.1126/science.1136466.

Kennedy, A. B., U. Gravois, B. C. Zachry, J. J. Westerink, M. E. Hope, J. C. Dietrich, M. D. Powell, A. T. Cox, R. A. Luettich Jr., and R. G. Dean (2011), Origin of the Hurricane Ike forerunner surge, *Geophys. Res. Lett.*, *38*, L08608, doi:10.1029/2011GL047090.

Kleiss, J. M., and W. K. Melville (2011), The analysis of sea surface imagery for white cap kinematics, *J. Atmos. Oceanic Technol.*, *28*(2), 219–243, doi:10.1175/2010JTECHO744.1.

Kraan, C., W. A. Oost, and P. A. E. M. Janssen (1996), Wave energy dissipation by white caps, *J. Atmos. Oceanic Technol.*, *13*, 262–267, doi:10.1175/1520-0426(1996)013<0262:WEDBW>2.0.CO;2.

Kudryavtsev, V. N., and V. K. Makin (2007), Aerodynamic roughness of the sea surface at high winds, *Boundary Layer Meteorol.*, *125*, 289–303, doi:10.1007/s10546-007-9184-7.

Kuik, A. J., G. P. Van Vledder, and L. H. Holthuijsen (1988), A method for the routine analysis of pitch-and-roll buoy wave data, *J. Phys. Oceanogr.*, *18*(7), 1020–1034, doi:10.1175/1520-0485(1988)018<1020:AMFTRA>2.0.CO;2.

Lafon, C., J. Piazzola, P. Forget, O. Le Calve, and S. Despiau (2004), Analysis of the variation of the whitecap fraction as measured in a coastal zone, *Boundary Layer Meteorol.*, *111*(2), 339–360, doi:10.1023/B:BOUN.0000016490.83880.63.

Lafon, C., J. Piazzola, P. Forget, and S. Despiau (2007), Whitecap coverage in coastal environment for steady and unsteady wave field conditions, *J. Mar. Syst.*, *66*, 38–46, doi:10.1016/j.jmarsys.2006.02.013.

Large, W. G., and S. Pond (1981), Open ocean momentum flux measurements in moderate to strong winds, *J. Phys. Oceanogr.*, *11*, 324–336, doi:10.1175/1520-0485(1981)011<0324:OOMFMI>2.0.CO;2.

Longuet-Higgins, M. S. (1957), The statistical analysis of a random, moving surface, *Philos. Trans. R. Soc. London, Ser. A*, *249*, 321–387, doi:10.1098/rsta.1957.0002.

Miller, B. I. (1964), A study of the filling of hurricane Donna (1960) over land, *Mon. Weather Rev.*, *92*(9), 389–406, doi:10.1175/1520-0493(1964)092<0389:ASOTFO>2.3.CO;2.

Monahan, E. C., and I. Ó Muircheartaigh (1980), Optimal power law description of oceanic white cap coverage dependence on wind speed, *J. Phys. Oceanogr.*, *10*, 2094–2099, doi:10.1175/1520-0485(1980)010<2094:OPLDOO>2.0.CO;2.

Moon, I.-J., I. Ginis, T. Hara, and B. Thomas (2007), A physics-based parameterization of air-sea momentum flux at high wind speeds and its impact on hurricane intensity predictions, *Mon. Weather Rev.*, *135*, 2869–2878, doi:10.1175/MWR3432.1.

Nordberg, W., J. Conaway, D. B. Ross, and T. Wilheit (1971), Measurements of microwave emission from a foam-covered, wind-driven sea, *J. Atmos. Sci.*, *28*, 429–435, doi:10.1175/1520-0469(1971)028<0429:MOMEFA>2.0.CO;2.

Petersen, G. N., and I. A. Renfrew (2009), Aircraft-based observations of air–sea fluxes over Denmark Strait and the Irminger Sea during high wind speed conditions, *Q. J. R. Meteorol. Soc.*, *135*, 2030–2045, doi:10.1002/qj.355.

Phillips, O. M. (1985), Spectral and statistical properties of the equilibrium range in wind-generated gravity waves, *J. Fluid Mech.*, *156*, 505–531, doi:10.1017/S0022112085002221.

Portilla, J., F. J. Ocampo-Torres, and J. Monbaliu (2009), Spectral partitioning and identification of wind sea and swell, *J. Atmos. Oceanic Technol.*, *26*(1), 107–122, doi:10.1175/2008JTECHO609.1.

Powell, M. D. (1980), Evaluations of diagnostic marine boundary-layer models applied to hurricanes, *Mon. Weather Rev.*, *108*(6), 757–766, doi:10.1175/1520-0493(1980)108<0757:EODMBL>2.0.CO;2.

Powell, M. D., P. J. Vickery, and T. A. Reinhold (2003), Reduced drag coefficient for high wind speeds in tropical cyclones, *Nature*, *422*, 279–283, doi:10.1038/nature01481.

Powell, M. D., et al. (2010), Reconstruction of hurricane Katrina's wind fields for storm surge and wave hindcasting, *Ocean Eng.*, *37*, 26–36, doi:10.1016/j.oceaneng.2009.08.014.

Reul, N., H. Branger, and J.-P. Giovanangeli (2008), Air flow structure over short-gravity breaking water waves, *Boundary Layer Meteorol.*, *126*, 477–505, doi:10.1007/s10546-007-9240-3.

Ross, D. B., and V. Cardone (1974), Observations of oceanic white caps and their relation to remote measurements of surface wind speed, *J. Geophys. Res.*, *79*(3), 444–452, doi:10.1029/JC079i003p00444.

Smith, S. D., and E. G. Banke (1975), Variation of the sea surface drag coefficient with wind speed, *Q. J. R. Meteorol. Soc.*, *101*, 665–673, doi:10.1002/qj.49710142920.

Soloviev, A., and R. Lukas (2010), Effects of bubbles and sea spray on air-sea exchange in hurricane conditions, *Boundary Layer Meteorol.*, *136*(3), 365–376, doi:10.1007/s10546-010-9505-0.

Sugihara, Y., H. Tsumori, T. Ohga, H. Yoshioka, and S. Serizawa (2007), Variation of whitecap coverage with wave-field conditions, *J. Mar. Syst.*, *66*, 47–60, doi:10.1016/j.jmarsys.2006.01.014.

Taylor, P. K., and M. J. Yelland (2001), The dependence of sea surface roughness an the height and steepness of the waves, *J. Phys. Oceanogr.*, *31*, 572–590, doi:10.1175/1520-0485(2001)031<0572:TDOSSR>2.0.CO;2.

Tennekes, H. (1973), The logarithmic wind profile, *J. Atmos. Sci.*, *30*, 234–238, doi:10.1175/1520-0469(1973)030<0234:TLWP>2.0.CO;2.

Tolman, H. L., and D. Chalikov (1996), Source terms in a third-generation wind wave model, *J. Phys. Oceanogr.*, *26*, 2497–2518, doi:10.1175/1520-0485(1996)026<2497:STIATG>2.0.CO;2.

Vickery, P. J., D. Wadhera, M. Powell, and Y. Chen (2009), A hurricane boundary layer and wind field model for use in engineering applications, *J. Appl. Meteorol. Climatol.*, *48*(2), 381–405, doi:10.1175/2008JAMC1841.1.

WAMDI group (1988), The WAM model—A third generation ocean wave prediction model, *J. Phys. Oceanogr.*, *18*(12), 1775–1810.

Wright, C. W., E. J. Walsh, D. Vandemark, W. B. Krabill, A. W. Garcia, S. H. Houston, M. D. Powell, P. G. Black, and F. D. Marks (2001), Hurricane directional wave spectrum spatial variation in the open ocean, *J. Phys. Oceanogr.*, *31*, 2472–2488, doi:10.1175/1520-0485(2001)031<2472:HDWSSV>2.0.CO;2.

Wu, J. (1982), Wind-stress coefficients over sea surface from breeze to hurricane, *J. Geophys. Res.*, *87*(C12), 9704–9706, doi:10.1029/JC087iC12p09704.

Zhang, J. A., P. G. Black, J. R. French, and W. M. Drennan (2008), First direct measurements of enthalpy flux in the hurricane boundary layer: The CBLAST results, *Geophys. Res. Lett.*, *35*, L14813, doi:10.1029/2008GL034374.

Zhao, D., and Y. Toba (2001), Dependence of white cap coverage on wind and wave properties, *J. Oceanogr.*, *57*, 603–616, doi:10.1023/A:1021215904955.

Zweers, N. C., V. K. Makin, J. W. De Vries, and G. Burgers (2010), A sea drag relation for hurricane wind speeds, *Geophys. Res. Lett.*, *37*, L21811, doi:10.1029/2010GL045002.